

The Effectiveness of a Distant Accelerometer Array to Compute Seismic Source Parameters: The April 2009 L'Aquila Earthquake Case History

by Nils Maercklin, Aldo Zollo, Antonella Orefice, Gaetano Festa, Antonio Emolo, Raffaella De Matteis, Bertrand Delouis, and Antonella Bobbio

Abstract The 6 April 2009 M_w 6.3 L'Aquila earthquake, central Italy, has been recorded by the Irpinia Seismic Network (ISNet) about 250 km southeast of the epicenter. Up to 19 three-component accelerometer stations could be used to infer the main source parameters with different seismological methods. We obtained an approximate location of the event from arrival times and array-based back-azimuth measurements and estimated the local magnitude (6.1) from an attenuation relation for southern Italy. Assuming an omega-square spectral model, we inverted S -wave displacement spectra for moment magnitude (6.3), corner frequency (0.33 Hz), stress drop (2.5 MPa), and apparent stress (1.6 MPa). Waveform modeling using a point source and an extended-source model provided consistent moment tensors with a centroid depth around 6 km and a prevalently normal fault plane solution with a dominant directivity toward the southeast. The relatively high corner frequency and an overestimated moment magnitude of 6.4 from moment tensor inversions are attributed to the rupture directivity effect. To image the rupture geometry, we implemented a beamforming technique that back-projects the recorded direct P -wave amplitudes into the earthquake source region. A northwest–southeast striking rupture of 17 km length is imaged, propagating with an average velocity up to 3 km/s. This value is significantly higher than our estimate of 2.2 km/s from S -wave spectra. Our case study demonstrates that the use of array techniques and a dense accelerometer network can provide quick and robust estimates of source parameters of moderate-sized earthquakes located outside the network.

Introduction

On 6 April 2009 a M_w 6.3 earthquake struck the Abruzzo region in central Italy and destroyed entire districts of the town of L'Aquila and of nearby settlements. The event caused more than 300 casualties and a series of building collapses in a region up to some 20 km away from the epicentral area, mainly in the southeast direction. The unexpected width of observed losses for such a moderate-sized event has triggered a heated debate in the media and public opinion. The earthquake ruptured a northwest–southeast active segment of the normal fault system embedded in the mountain front of the central Apennines (Cirella *et al.*, 2009; Walters *et al.*, 2009). This normal faulting structure shows extension perpendicular to the Apennines trend, which is consistent with the Quaternary tectonics of the internal sector of the belt (Galadini and Galli, 1999). A general view on the seismicity in the study region is given in Bagh *et al.* (2007). More specifically,

Di Luccio *et al.* (2010) discuss the foreshocks and aftershocks of the L'Aquila earthquake in relation to geodynamic issues.

A rapid estimation of earthquake source parameters can be highly relevant for civil protection operations after an event. Distant, dense accelerometer networks with real-time data transmission and considered as an array can provide reliable information on the main source parameters. This is especially relevant when near-source data are not readily available. In this paper, we demonstrate the feasibility of this approach in the case of the L'Aquila earthquake. In particular, we describe and discuss the event location procedure, the accurate estimation of local and moment magnitude, and moment tensor inversions for point sources and for an extended-source model. At the end we focus on extended-source properties such as rupture length, strike, and rupture velocity. All these analyses can be implemented in an

automatic, near-real-time processing sequence for the considered array of stations.

Data

The Irpinia Seismic Network (ISNet, Fig. 1) is a dense, local seismographic network in the Campania–Lucania region in southern Italy (Weber *et al.*, 2007). The network features 28 seismic stations organized in four subnets. Stations of a given subnet are connected with real-time communications to a local control center. These centers are linked to each other and to a central network control center, permitting the determination of earthquake source parameters within

a short time after the event. Each ISNet station is equipped with two three-component instruments, a Guralp CMG-5T strong-motion accelerometer and a short-period velocimeter (Geotech S-13J). Five stations host broad-band 40-s velocimeters instead of the short-period instruments for a better recording of regional and teleseismic events (Nanometrics Trillium 40s). The entire array has an aperture of about 70 km times 90 km, and its center is located about 250 km southeast of the epicenter of the L'Aquila earthquake.

The L'Aquila earthquake has been recorded in real time by 19 ISNet stations. Figure 2 (left) shows the vertical-component acceleration records for this event. The traces

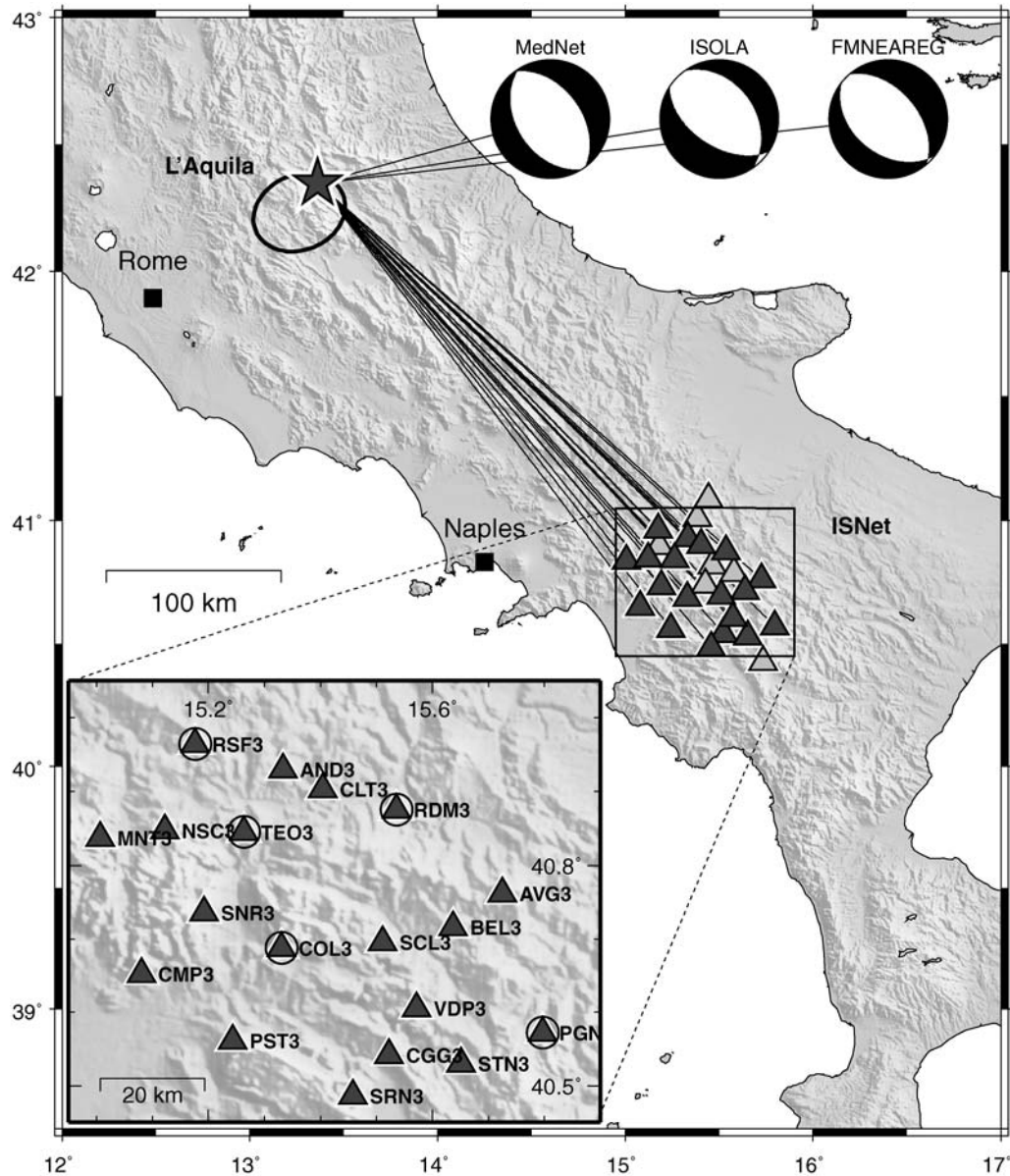


Figure 1. Map of the ISNet array (triangles) and the L'Aquila earthquake (star). The ellipse marks the epicenter of the event as obtained only from ISNet stations (90% confidence). Focal mechanisms for the L'Aquila earthquake determined in this study (using ISOLA and FMNEAREG methods) are shown together with the MedNet solution. The inset map shows those ISNet stations that recorded the event, and circles indicate the locations of additional ISNet broad-band seismometers.

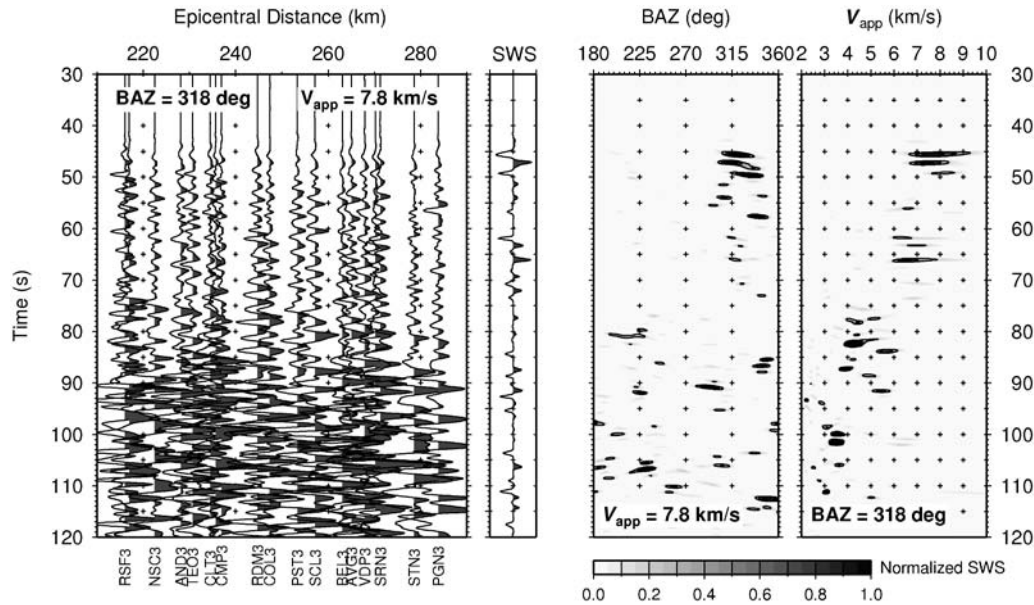


Figure 2. (Left) Vertical-component acceleration records and beam analysis panels used to determine (right) back azimuths (BAZ) and apparent velocities (V_{app}) of incoming waves. The traces are low-pass filtered below 0.5 Hz, amplitude-normalized, sorted by epicentral distance, and aligned according to the given beam parameters. SWS denotes a semblance-weighted stack. The beam analysis panels show the normalized SWS amplitude for different back azimuths and a constant apparent velocity and for different velocities and constant back azimuth, respectively.

are 0.5-Hz low-pass filtered, normalized to the maximum amplitude of each trace, and sorted by epicentral distance. For display, the traces are aligned using delay times computed for a plane wave arriving from a back azimuth of 318° and with an apparent velocity of 7.8 km/s (e.g., Rost and Thomas, 2002). In this seismic section, the first P -wave arrival is at about 45 s for all traces. To account for elevation differences and local velocity variations, P -wave station corrections, which have been determined from local events inside the ISNet array, have been applied.

The recorded, low-pass filtered waveforms are very coherent and permit the application of array processing methods to measure back azimuth and slowness of the incoming waves. Delay times relative to a reference station depend on the back azimuth and the slowness or apparent velocity of the seismic phase of interest (e.g., Rost and Thomas, 2002). Figure 2 (right) shows back azimuth and apparent velocity observed at ISNet as a function of time in terms of the stack amplitude weighted by the semblance waveform coherency measure (Neidell and Taner, 1971). In each of these two beam analysis panels, one of the two beam parameters to compute delay times is held fixed, while the other one is varied. The left panel shows back azimuths for a constant apparent velocity of $V_{app} = 7.8$ km/s, while the right panel shows the apparent velocities for a constant back azimuth of 318° . The reference station is COL3 near the center of the ISNet array. The first P -wave arrivals are characterized by an apparent velocity near 8 km/s, as indicated by dark regions at 45–50 s in the velocity analysis panel on the right (vespagram; e.g., Rost and Thomas, 2002). Some

later coherent phases with lower apparent velocities are visible at later times, and a significant decrease of apparent velocities near 75 s indicate the direct S -wave arrival. The observed back azimuth (BAZ) of the first P -wave arrivals is 318° , with an uncertainty of some $\pm 5^\circ$. Without an application of station corrections, the measured P -wave back azimuth would be about 314° .

Location and Magnitude

Hypocentral locations of the L'Aquila earthquake have been reported by various agencies (e.g., Walters *et al.*, 2009). From our own, manually picked P -wave and S -wave arrival times at near-source accelerometric stations of the National Accelerometric Network (RAN; Rete Accelerometrica Nazionale), operated by the Italian Department of Civil Protection, we determined the hypocenter at 42.3479° N, 13.3542° E and 8-km depth (hereafter called the reference location). This location is close to the reported locations of the various agencies. Here we give some notes on the feasibility to locate regional events when considering ISNet as a single array or seismic antenna.

Given an appropriate velocity model, a seismic event can be located by a single station at which P -wave and S -wave arrival times and the back azimuth have been measured (e.g., Frohlich and Pulliam, 1999). We use a one-dimensional (1D) regional velocity model for central Italy (model III in Li *et al.*, 2007), and the P -wave and S -wave arrival times at the reference station COL3 (i.e., the P -wave arrival at 01:33:19.45 UTC and an S - P travel time difference of 29.5 s). The P -wave back azimuth of 318° is estimated

from beam analysis panels as described previously in this paper. To locate the event, we applied the HYPOSAT routine (Schweitzer, 2001), which utilizes both the arrival times and the back azimuth to obtain the hypocenter solution with a generalized matrix inversion method.

Fixing the event depth to 10 km, we find the epicenter location at $42.2993^\circ\text{N} \pm 0.2041^\circ$, $13.3553^\circ\text{E} \pm 0.2820^\circ$ and the origin time at $01:32:43.923\text{ UTC} \pm 2.11\text{ s}$. The epicenter error ellipse with 90% confidence is plotted in Figure 1. This epicenter location is about 5.5 km west–southwest of our reference solution as obtained from the local RAN data. The chosen regional velocity model is appropriate for this source–receiver path, because the epicentral distance from the reference station COL3 is only 4 km shorter than the distance to the reference location. The azimuthal deviation from the reference location is mostly due to the small error of 1° in our back-azimuth estimate of 318° , compared with the reference back azimuth of 319° from local data. The two largest aftershocks of the L’Aquila mainshock show the same back-azimuth deviation. This observation is most likely caused by crustal velocity variations beneath the ISNet array that are not accounted for by the station corrections used, or the back-azimuth deviation may also be related to crustal heterogeneities along the ray path from the array to the event.

Local Magnitude

The local magnitude is a measure of the source size through the high-frequency content of the radiation emitted by a fault during a seismic event, properly corrected for the source–station distance. For southern Italy, the local magnitude corresponding to a Wood–Anderson peak displacement A , recorded at hypocentral distance R , can be computed from the relation

$$M_L = \log A + 1.79 \log R - 0.58 \quad (1)$$

(Bobbio *et al.*, 2009). In this equation A is measured in millimeters and R in kilometers, and the error associated with a single estimate of M_L can range between 0.1 and 0.3, depending on the accuracy of the location. The error decreases as the distance increases. To obtain synthetic Wood–Anderson waveforms, strong-motion data are twice integrated and convolved with the Wood–Anderson response. On a single horizontal component, the peak displacement is computed as half the maximum of the peak-to-peak displacement on the Wood–Anderson synthesized record, and the value A to be used for the magnitude estimation is the arithmetic mean of peaks measured on both horizontal components. Finally the local magnitude is the Huber mean (Huber, 1964) of the single-station magnitude values. The Huber mean utilizes weighting factors to downweight the influence of outliers on the final magnitude estimation.

Although equation 1 has been derived for small magnitude events ($M_L < 3.5$) that occurred along the Apennine chain in southern Italy, it is routinely used by the automatic

system processing the data of ISNet, and it also provided the magnitude of the 6 April L’Aquila earthquake. The value of the magnitude at each array station is shown in Table 1, and the contribution to the data distribution is represented in Figure 3 with black blocks. In the histogram, we fix a bin width of 0.2 magnitude units, which is comparable to the error associated with the single-station magnitude estimation. Accelerometric estimations of local magnitude mostly gather in the bin ($6.0 \leq M_L < 6.2$), resulting in a Huber mean of $M_L = 6.08 \pm 0.17$.

Also, the 55 available three-component accelerometric stations of the RAN network between 10 km and 280 km hypocentral distance allowed for correct computation of the local magnitude. *De facto*, whatever decay relationship is used to describe the attenuation of the peak with the distance, it has a fixed point at 100 km imposed by the constraint that $M_L = 3$ when $A = 1$. Hence, at receivers close to the reference distance, we expect that the differences in the local magnitude obtained using different attenuation relationships are small when compared to the variability of the single magnitude estimate.

We selected six RAN stations in the distance range 70–130 km from the hypocenter, and we processed the accelerometric data as previously described in this paper for the computation of the Wood–Anderson peak displacement, resulting in M_L 6.11, when using the southern Italy attenuation relationship. If we used the Hutton and Boore (HB) magnitude relationship (Hutton and Boore, 1987), currently employed by the Istituto Nazionale di Geofisica e Vulcanologia (INGV) for the computation of the local magnitude in Italy (Amato and Mele, 2008), we would get an M_L 6.09. Therefore, the effective local magnitude of the event is 6.1, and this value is very consistent with the one provided by equation 1 and the data of ISNet. It is worth noting that equation 1 applied to the whole RAN dataset still provides a local magnitude of 6.1. The magnitude distribution from RAN data is superimposed in gray on Figure 3 and shows the same trend, with a bit larger maximum value and few data on the tails of the distribution. Such a comparison indicates that ISNet data are effectively representative of the average high frequency radiated by the earthquake.

The application of the HB relationship on the RAN data yields M_L 6.2, while the restriction to the ISNet data leads to the smaller value M_L 5.8, which is the local magnitude

Table 1
Magnitude Estimates for Single Stations of ISNet*

Station	M_L	Station	M_L	Station	M_L	Station	M_L
AND3	6.27	CMP3	6.12	PST3	5.82	SRN3	5.85
AVG3	6.16	COL3	6.09	RDM3	6.39	STN3	6.16
BEL3	6.23	MNT3	5.82	RSF3	6.14	TEO3	6.27
C GG3	5.99	NSC3	6.02	SCL3	5.93	VDP3	6.04
CLT3	6.14	PGN3	5.81	SNR3	6.18		

*See Figure 1. The magnitude ranges between 5.81 and 6.27, with most data gathering in the range 6.0–6.2.

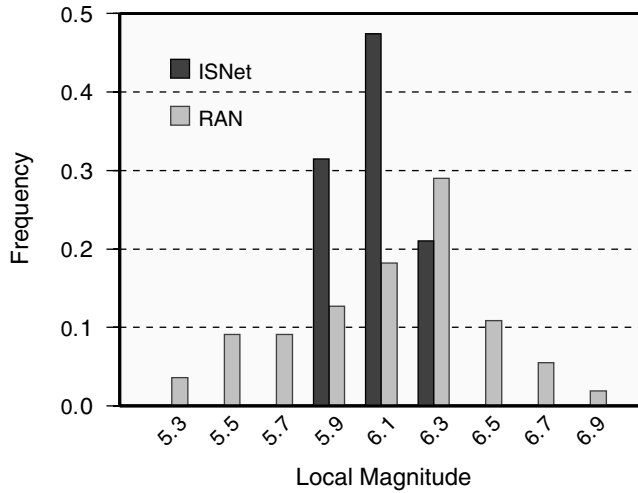


Figure 3. Histogram of the magnitude distribution for the L'Aquila earthquake determined from the data of ISNet (black) and RAN (gray). The data are normalized to show the occurrence frequency of the single networks. The bin width is 0.2 and is comparable with the error on the single-station magnitude estimates.

officially declared by the INGV. Although equation 1 fits data in a different magnitude range, it performed better than HB on ISNet data, indicating that regionalization of attenuation relationships is a necessary step for a correct estimate of the local magnitude. When magnitude relationships are not calibrated on the region of interest, a combination of data recorded at distances smaller and larger than those of the reference distance are likely to better resolve underestimation and overestimation of the magnitude.

Moment Magnitude, Rupture Velocity, and Stress Release Estimates

The P -wave and S -wave displacement spectra obtained from the 19 three-component accelerometric and 5 broadband records were inverted to determine the main source parameters. We assumed an omega-square spectral model

$$S(\omega) = \frac{\Omega_0}{1 + \left(\frac{\omega}{\omega_c}\right)^2} e^{-\omega t^*} \quad (2)$$

with the parameter $t^* = T/Q$, in which T denotes the travel time and Q the frequency-independent quality factor. The parameter t^* was estimated directly from the high-frequency spectral decay for S waves, as measured at all the ISNet stations, along with the low-frequency spectral level Ω_0 and the angular corner frequency $\omega_c = 2\pi f_c$. The P - and S -displacement spectra from velocity and acceleration sensors were inverted using the nonlinear Levenberg–Marquardt least-square algorithm for curve fitting (Marquardt, 1963).

After the visual inspection of the S -wave acceleration spectra, we restricted our source and path attenuation analysis to a maximum frequency of 2 Hz because of the well-known sharp change of the spectral decay at higher fre-

quencies, which is likely the result of attenuation effects of near-source weathered layers (Anderson and Hough, 1984). Initially we estimated the value of $t^* = 0.17 \pm 0.09$ by averaging the measurements obtained from the inversion of the displacement spectra. Taking an average S -wave travel time of $T = 70$ s, this value leads to a quality factor of $Q_S = 412 \pm 218$, which is an average value of the S -attenuation parameter for the whole volume that encompasses the region from the source to the ISNet stations. The subsequent inversions to determine the parameters Ω_0 and ω_c are performed with a fixed value of $t^* = 0.17$ s, both for P and S waves.

Estimates of the seismic moment from each displacement spectrum are obtained through the equation

$$M_0 = \frac{4\pi\rho_0^{1/2}\rho_Z^{1/2}V_0^{5/2}V_Z^{1/2}R_S}{F_S R_{\Theta\phi}} \Omega_0 \quad (3)$$

for a vertically heterogeneous velocity medium (Aki and Richards, 1980), in which ρ is the density and V is the P -wave or S -wave velocity. Subscripts 0 and Z for density and velocity indicate the values at the Earth's surface and at the source depth, respectively. Here we used a constant-gradient local crustal model, approximating the 1D layered model in Bagh *et al.* (2007), with $\rho_0 = \rho_Z = 2700$ kg/m³, $V_{0P} = 5.2$ km/s, $V_{0S} = 2.9$ km/s, $V_{ZP} = 5.6$ km/s, and $V_{ZS} = 3.1$ km/s. The variable $R_{\Theta\phi}$ in equation 3 is the average radiation pattern coefficient (0.62 for P waves and 0.52 for S waves), and $F_S = 2$ accounts for the free-surface amplification. The geometrical spreading factor R_S is computed for an approximate 1D velocity model, where velocity is linearly related to the depth.

From the S -wave displacement spectra shown in Figure 4, we estimated a seismic moment of $M_0 = 3.1 \pm 0.09 \times 10^{18}$ N m. This estimate is consistent with the value computed from P waves ($1.8 \pm 0.05 \times 10^{18}$ N m) within a factor of 1.7, providing a moment magnitude

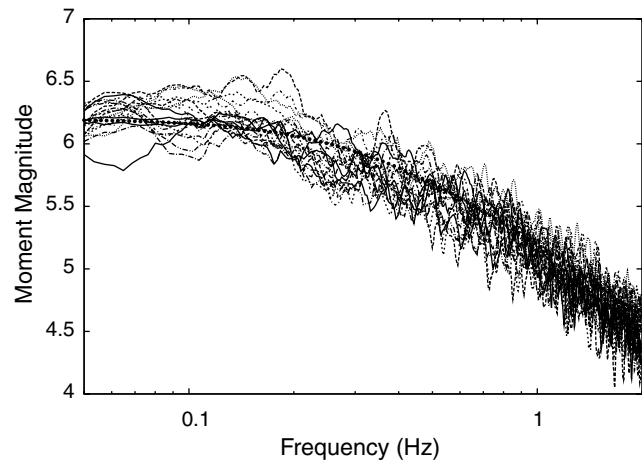


Figure 4. Overlay of all S -wave displacement spectra observed at ISNet accelerometer stations (gray dashed and solid lines). The black dotted line is the displacement spectrum for the best-fit model.

$M_w = 6.2 \pm 0.1$. This value is also consistent with the local magnitude M_L 6.1 inferred from Wood–Anderson synthetic records (see [Local Magnitude](#) section).

The spectral inversion provides a relatively high average S -wave corner frequency of $f_c = 0.33 \pm 0.06$ Hz, which is attributed to an enhanced rupture directivity effect toward the array. To estimate the rupture velocity, we assume a southeast propagating rupture (Cirella *et al.*, 2009) with a total length $L = 17$ km as inferred from the rupture tracking analysis (see [Kinematic Rupture Tracking](#) section). Then the measured S -wave corner frequency yields an average rupture velocity of $v_r = 2.2$ km/s through the relation

$$f_c = \frac{v_r}{L} \left(1 - \frac{v_r}{V_S} \cos(\phi) \right)^{-1}. \quad (4)$$

In this equation, $\phi = 3^\circ \pm 3^\circ$ is the directivity angle between the rupture direction and the S ray leaving the source, and $V_S = 3.4$ km/s is the mean S velocity along the ray path from the hypocenter to the ISNet array.

For a rectangular fault with length L and width W , an estimate of the static stress drop can be obtained from the seismic moment and rupture length using the relationship

$$\Delta\sigma = \frac{M_0}{\alpha^2 L^3}, \quad (5)$$

in which the aspect ratio $\alpha = W/L$ is fixed at $\alpha = 0.5$ in the present case. This relationship is derived from the solution by Madariaga (1977a, 1977b) for the general problem of a shear crack under an uniform stress drop. In our case of the L'Aquila earthquake, we obtain a static stress drop value of $\Delta\sigma = 2.5 \pm 1.1$ MPa.

Wyss (1970) proposed an independent estimation of stress release (apparent stress) that can be obtained from the measurements of seismic moment and radiated energy E_S via

$$\tau_a = \mu \frac{E_S}{M_0}, \quad (6)$$

where μ is rigidity. According to Madariaga (1976) and Boatwright (1984), the apparent stress is a proxy for the dynamic stress release, that is the difference between the initial stress and the residual fault strength during rupture propagation. Following Boatwright (1980), we estimated the radiated S -wave energy from the integral of the squared velocity as computed from the velocity spectra and using Parseval's theorem Snoko (1987).

We obtained an average value of $E_S = 1.7 \pm 1.7 \times 10^{14}$ J for the radiated S -wave energy after spectral correction for anelastic attenuation and instrument frequency bandwidth (Ide and Beroza, 2001). This value for E_S leads to an apparent stress estimate of $\tau_a = 1.6 \pm 0.8$ MPa, which is very consistent with our static stress release estimate.

Moment Tensor

We use two different approaches to infer some insights about the L'Aquila earthquake fault plane solutions and moment tensor from the inversion of strong-motion data recorded at the ISNet stations. The first method, which is named ISOLA (ISOLated Asperities), was developed by Sokos and Zahradník (2008). It is based on the point-source approximation and performs a grid search over a set of trial source positions and time shifts in order to identify the optimal centroid position and time and the moment tensor components through a minimization of the residual errors obtained from the comparison of synthetic and observed complete waveforms. This procedure is equivalent to maximizing the correlation between real and synthetic seismograms. The ISOLA code uses instrumentally corrected seismograms. In general, to avoid errors related to the poor knowledge of the propagation medium, relatively low frequencies should be selected in the data, keeping in mind that, in several cases, the long-period signal content might be contaminated by instrumental and/or natural noise. For this reason, data must be carefully processed and inspected in order to identify the usable records and the best frequency range in which the inversion should be performed. The present version of the ISOLA software is not ready for the automatic calculations (see [Data and Resources](#) section). Once the fault plane solution and the centroid position have been identified, it also is possible to gain some insights about the identification of the fault plane with respect to the auxiliary plane. To this end, the hypocenter–centroid (Zahradník *et al.*, 2008) can be used when hypocentral earthquake location and centroid moment tensor solution are both available. Considering two planes passing through the centroid, and having strike and dip of the moment tensor solution, the fault plane is the one encompassing the hypocenter.

The second method, named FMNEAREG (Focal Mechanism from NEAR source to REGional distance records; Delouis *et al.*, 2008), is a fast grid search for double-couple solutions, based on a simple finite-dimension source representation and on the modeling of the complete displacement wave field. The source model is composed of point sources aligned along the strike of the fault plane. The length of the model depends on magnitude and is twice the dimension estimated using the empirical relation proposed by Wells and Coppersmith (1994). This allows the rupture to propagate bilaterally or unilaterally in the direction required by data. The number of point sources and their spacing increase with magnitude. Each point source is characterized by a local source time function, represented by six overlapping isosceles triangles, a time lag, and a slip angle (rake). The time lag (i.e., the rupture onset time) of each point source is relative to the earthquake origin. The acceleration records are integrated twice and band-pass filtered in a range that is automatically selected. An automated algorithm, introduced in Delouis *et al.* (2009) for the computation of moment magnitude from strong-motion records, is used to define

an effective high-pass cutoff frequency for each component of the seismogram. Moreover, the low-pass cutoff frequency is estimated using an empirical relation depending on magnitude and hypocentral distance; according to this relation, the maximum frequency decreases with both magnitude and distance. The filtered displacement recordings are inverted to find the parameters of the focal mechanism using a two-step grid search. In the first step, the minima of the normalized rms error between the observed data and the synthetics are searched using a coarse grid, while in the second step the search is performed in a finer grid around the minima previously identified. For each tested triplet (strike, dip, rake), the parameters of the point sources (amplitudes of the elementary triangular functions, rupture onset time, and rake) are determined through a simulated annealing algorithm.

ISOLA provides a full description of the moment tensor and allows the identification of the fault plane with respect to the auxiliary plane, while FMNEAREG only searches for a fault plane solution but has the advantage of automatically selecting the frequency ranges for each station and providing some insights on the moment distribution along the fault strike.

We used data from 17 three-component strong-motion stations of the ISNet network. In both approaches, the Green's functions are computed through the discrete wavenumber technique (Bouchon, 1981) in a 1D layered propagation medium. Thus, the full wave field is considered, and the methods are suitable for applications to regional and local events. In this work, we used the crustal model proposed by (Bagh *et al.*, 2007). Data have been inverted in a frequency range that spans a maximum frequency range of 0.02–0.06 Hz. The bandwidth used for each individual trace has been adjusted based on a fit of its acceleration spectra to an omega-square model to reject those parts with significant deviations. The mean low-cut frequency is 0.03 Hz.

The main results obtained are summarized in Table 2, and a comparison between observed and synthetic displacements obtained by both techniques is shown in Figure 5. The fault plane solution corresponds to a normal fault with a small strike component, and plane 1 has been identified as the fault plane (Table 2). This plane strikes approximately in the apenninic direction and dips toward the southwest.

From the moment tensor inversion, we find a centroid located at a 5-km depth beneath the epicenter. The seismic moment for the earthquake is about 5.8×10^{18} Nm, which corresponds to a moment magnitude of about M_w 6.4. This overestimation could be associated with the particular position of the ISNet station. In fact, the stations are located southeast of the earthquake and thus are influenced by the forward directivity effect. The double-couple percentage is about 94.5%. Different tests were performed using different hypocentral depths in the inversion by FMNEAREG, with the best solution at a focal depth of about 7 km. The relative seismic moment for each of the five source points aligned along the fault strike appears to be predominantly released towards the southeast direction (Fig. 6a), and then the rupture propagation is prevalently unilateral.

Kinematic Rupture Tracking

As shown in the Data section, the recorded low-pass filtered waveforms are very coherent and permit the application of array methods to measure back azimuth and slowness of the incoming waves (Fig. 2). Figure 6b further illustrates the waveform coherency after alignment at the first P -wave arrival, based on manual arrival time picks. To track the propagating rupture front of the event, we implemented a modified beamforming and stacking technique that back-projects the direct P -wave amplitudes recorded at the ISNet array into the earthquake source region. Similar back-projection techniques have been used, for example, to track the rupture of the great M_w 9.3 Sumatra–Andaman earthquake in space and time (Ishii *et al.*, 2005; Krüger and Ohrberger, 2005).

The rupture tracking procedure can be outlined as follows. First, define a grid of possible source locations in the region of the event to be imaged; and, for each defined grid point and each array station, compute travel times in an appropriate Earth model or the delay times relative to a reference station within the array. Second, stack the aligned traces of all array stations in a short time window around the computed time, and assign the stack amplitude or energy to the current grid point. An ordinary stack (i.e., the sum of all traces) or a stack weighted by waveform coherency (such as the semblance; Neidell and Taner, 1971) may be used here.

Table 2
Fault Plane Solutions Obtained by Both Techniques Adopted in This Work*

		Strike	Dip	Rake	Mrr	Mtt	Mpp	Mrt	Mrp	Mtp
		(degrees)			$(\times 10^{18}$ Nm)					
ISOLA	plane 1	123	53	−104	−5.4	2.8	2.6	−1.7	0.13	−3.1
	plane 2	325	40	−73						
FMNEAREG	plane 1	128	41	−99						
	plane 2	320	50	−82						

*From the inversion of the strong-motion data recorded at ISNet (see also Fig. 1). For the ISOLA method, the components of the moment tensor are also reported; they resulted in a double-couple percentage of 94.5%.

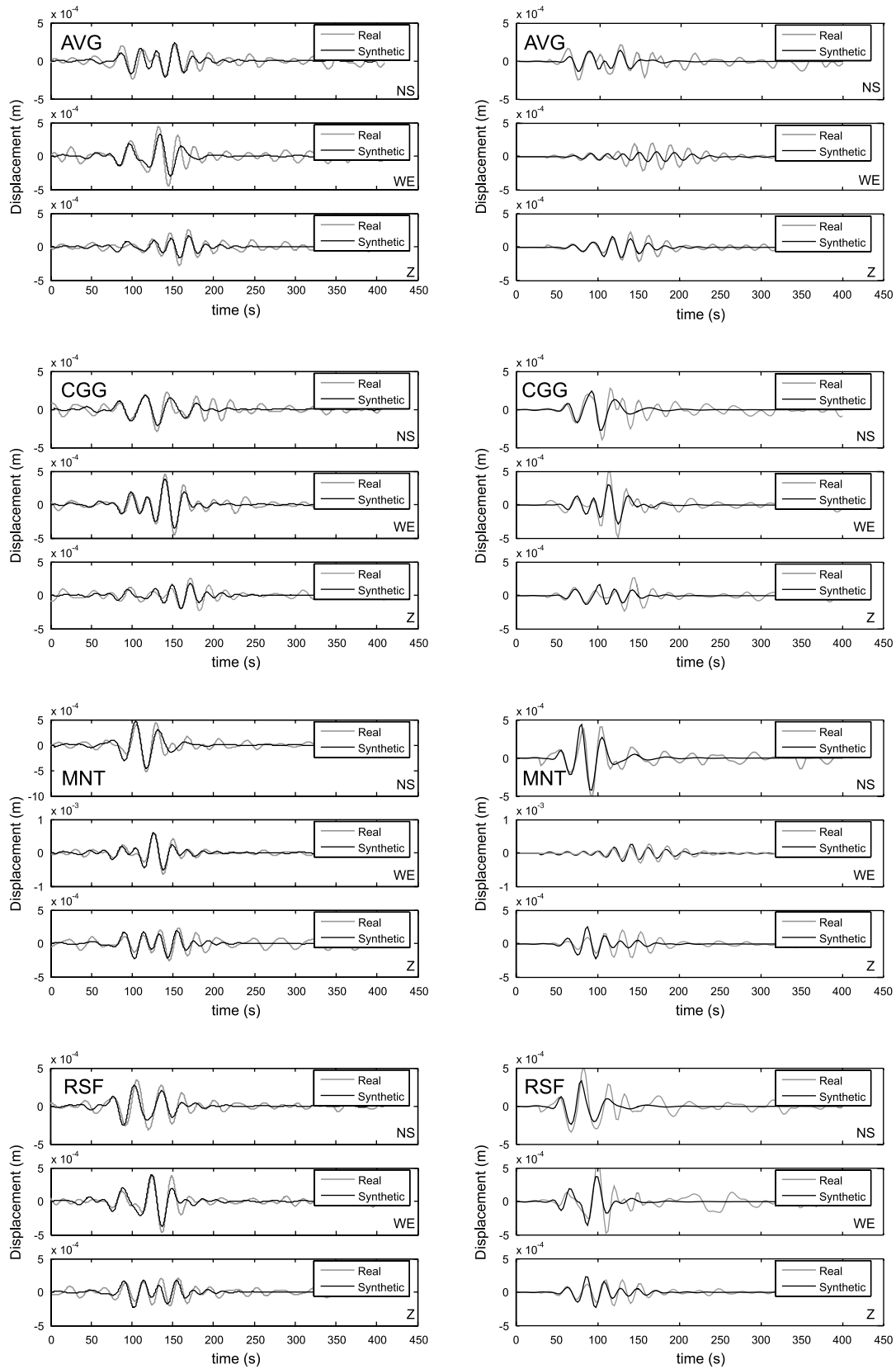


Figure 5. Some displacement seismograms obtained from ISNet strong-motion data (black lines) are compared with the synthetic waveforms (gray lines) computed by (left) ISOLA and (right) FMNEAREG. All seismograms are band-pass filtered within a maximum frequency range of 0.02–0.06 Hz. Note that the applied filters are not the same for the individual traces and inversion methods. The frequency range has been determined individually for each trace based on data quality.

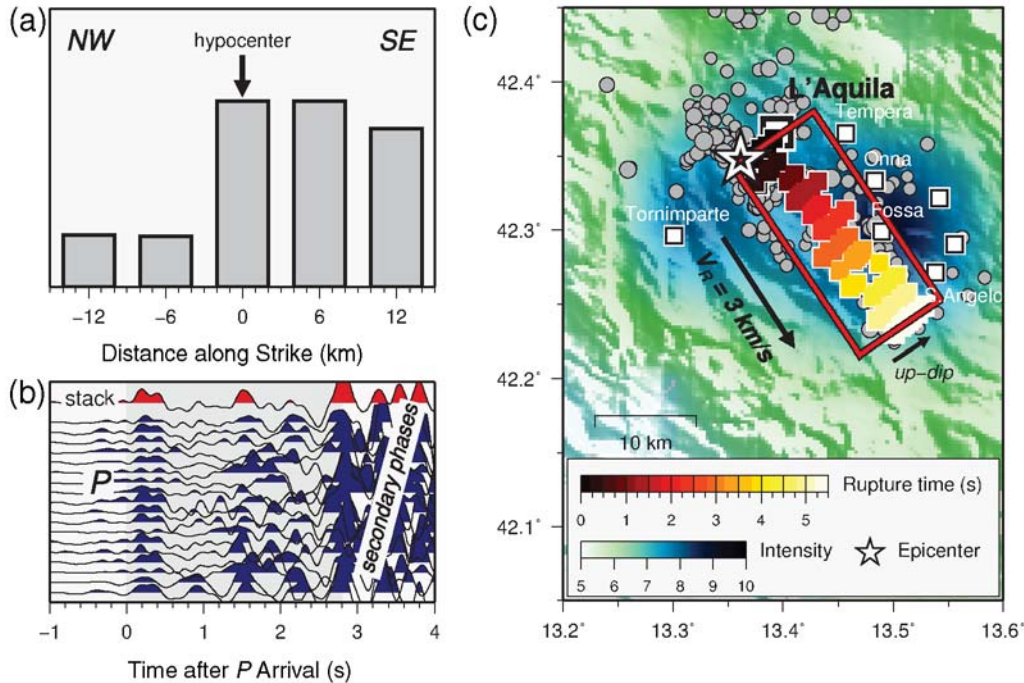


Figure 6. Results for an extended-source model. (a) Normalized distribution of the seismic moment along the fault strike (FMNEAREG). The five point sources are distributed on a trial source line of 30 km that is twice the fault length estimated by the Wells and Coppersmith (1994) relationship. (b) Vertical-component acceleration records, 0.25–4.0 Hz band-pass-filtered, amplitude-normalized, and sorted by epicentral distance. (c) Space–time evolution of the source from kinematic rupture tracking. Circles indicate $M > 3$ earthquakes in 2009, the box outlines the surface projection of the fault plane, and background colors illustrate the Mercalli–Cancani–Sieberg (MCS) intensity of the mainshock MCS data from Camassi *et al.* (2009).

Third, mark the location of the stack maximum in the source region. Finally, repeat this process in a moving time window along the entire time segment of interest; for example, the P coda. The result is an image of the space–time distribution of the sources of energy observed in a seismogram.

To track the rupture of the L’Aquila earthquake, we used 0.02–2 Hz band-pass-filtered vertical-component acceleration records from the 19 stations that recorded the event (Fig. 1). Initially, we defined a regular grid of possible source locations in a volume of 100 km \times 100 km \times 15 km around the hypocenter. Because initial tests showed that our procedure does not provide significant depth resolution, we later restricted our analysis to a horizontal grid with 0.25-km spacing, fixed at a depth of 8 km. Travel times were computed from each station to each grid node, assuming a constant average velocity of 6.1 km/s from the source to the ISNet stations, and for a 1D regional crustal velocity model (Li *et al.*, 2007). After the application of elevation static corrections with a replacement velocity of 2.5 km/s, we aligned the traces according to the computed times and stacked the traces weighted by the semblance. We measured the semblance-weighted stack amplitudes in a 0.5-s sliding time window along the seismogram with a time step of 0.25 s. The amplitude measurements started at the time of the first P -wave arrival. The end of the analysis window was given by the time corresponding to the arrival of scattered and multipath secondary phases, which are imaged at locations not consis-

tent with the location obtained in the previous time step. The total, usable length of the analysis time window is 2.8–3.0 s, which may not cover the entire apparent source time function theoretically observable at ISNet.

Given the specific acquisition layout, our beamforming method is not able to retrieve accurate absolute location and hypocenter depth, while relative location errors are smaller than 2 km. Taking the locations of the semblance-weighted stack maxima for the different time steps, we obtain a rupture direction of N142° E (Fig. 6c), which is consistent with the main fault strike. The imaged rupture zone is about 17 km long (colored strip in Fig. 6c), and the rupture propagates unilaterally from northwest to southeast. For display, the entire rupture image shown in Figure 6c has been shifted laterally from the location obtained from ISNet to the better epicenter solution obtained from local data (star).

The mean apparent rupture velocity v_r^a is given by the rupture length divided by the corresponding time segment on the observed seismograms (i.e., the apparent source time function). Here we used the entire analysis window of 2.8 s as defined previously in this paper. To obtain the true rupture velocity v_r , the directivity effect has to be taken into account via

$$v_r = \frac{v_r^a}{1 - \frac{v_r^a}{V_p} \cos \phi}, \quad (7)$$

with the P -wave velocity $V_P = 6.1$ km/s and the directivity angle $\phi = 3^\circ$. This provides a rupture duration of 5.6 s and a mean rupture velocity of 3 km/s, corresponding to slightly less than 90% of shear wave velocity in the source region. The color-coded times in Figure 6c correspond to the source–time function corrected for directivity.

Discussion and Conclusions

We considered the Irpinia Seismic Network as an array or seismic antenna with the aim to quickly estimate source parameters of an event outside the network. For the April 2009 L'Aquila earthquake, we obtained an approximate location, estimated magnitude values and moment tensors, and imaged rupture geometry and velocity. The individual seismological methods applied here and the results are discussed in [Location and Magnitude](#), [Moment Tensor](#), and [Kinematic Rupture Tracking](#) sections.

Our analyses focused on the ISNet acceleration records because these provide the required low-frequency content of the wave field and a high station density. Arriving phases are coherent across the accelerometer array. The five broadband sensors, each colocated with an accelerometer (Fig. 1), served as a reference to validate our results from accelerometric data. After single integration of acceleration records to get velocity, we compared these data with the broadband waveforms in different frequency bands. We always found identical waveforms for the two instrument types for frequencies down to at least 0.04 Hz, while the exact value may be lower and depends on data quality and on the actual filter parameters. A comparison of displacement spectra indicated the same general low-frequency limit for the ISNet accelerometers. The use of lower frequencies for the moment tensor inversion has been justified individually for each trace by a comparison of the acceleration spectrum with an omega-square source model.

An accurate location of an event outside an array requires an accurate velocity model and back-azimuth measurement in addition to arrival time picks. The high waveform coherency below 0.5 Hz for the L'Aquila earthquake recorded at ISNet accelerometers provided a good back-azimuth estimate from standard beamforming ([Rost and Thomas, 2002](#)). In spite of a rather large error ellipse (Fig. 1), the epicenter solution from ISNet data alone is close to the reference location from local stations. To improve the location capability of ISNet for regional events, refined station corrections for local heterogeneities and possibly azimuth corrections are needed. Only minor adjustments seem to be necessary for the adopted velocity model (model III in [Li et al., 2007](#)). However, it should be noted that none of the analyses applied in the present study requires a more accurate location than the solution we got from ISNet data.

From ISNet acceleration records and from local data (RAN), we estimate a consistent value of M_L 6.1 for the local magnitude, using a recently developed magnitude relationship for southern Italy (equation 1; [Bobbio et al., 2009](#)).

An application of the [Hutton and Boore \(1987\)](#) relationship, originally developed for southern California, yields a significantly lower value (M_L 5.8), illustrating the importance of regional calibration of local magnitude scales. Our moment magnitude estimate of M_W 6.2 from S -wave displacement spectra agrees well with results from previous seismological and from InSAR studies (e.g., [Walters et al., 2009](#)), whereas the moment tensor inversions lead to a higher value of M_W 6.4. This overestimation is attributed to the directivity effect, where ISNet is located roughly in the direction of rupture propagation (see Fig. 1).

The inversion of S -wave displacement spectra also resulted in a corner frequency of $f_c = 0.33$ Hz, a stress drop of $\Delta\sigma = 2.5$ MPa from fault length and seismic moment (equation 5), and an apparent stress of $\tau_a = 1.6$ MPa. Again, we relate the relatively high corner frequency to the rupture directivity effect. The values of stress drop and apparent stress are very similar. According to [Beeler et al. \(2003\)](#), this result ($\tau_a/\Delta\sigma \approx 1$) would imply a large negative stress overshoot (undershoot), which is an evidence for extreme dynamic weakening due to, for example, pore fluid pressurization or frictional melting. The shear resistance falls to zero, and all the energy is radiated. The role of fluids in the faulting processes of the L'Aquila earthquake sequence is also discussed in [Di Luccio et al. \(2010\)](#).

The use of the full waveforms in the moment tensor inversions permitted the retrieval of correct moment tensor solutions, even with the poor azimuthal coverage of the focal plane by ISNet stations. The optimum centroid depths are 5 km (ISOLA) and 7 km (FMNEAREG). The moment tensor solutions are consistent (Table 2) and agree with the previously published values (e.g., [Walters et al., 2009](#)). We found strike angles of 123° from ISOLA and 128° from FMNEAREG. On the other hand, kinematic rupture tracking shows a larger strike angle of about 142° . This angle agrees well with the strike from InSAR interferograms and the strike direction suggested by the geomorphology from satellite imagery (140 – 145° ; [Walters et al., 2009](#)). The discrepancy may be partly explained by a trade-off between the strike and the rake angle of the moment tensors. A change of the strike may be compensated by a change of the rake without a significant change of data fit.

In addition to the strike angle, the rupture image (Fig. 6c) constrains the fault length and rupture velocity, solely assuming a velocity model and waveform coherency across the array. The maximum source time after the P -wave arrival is given by a drop of waveform coherency or when imaged locations are not consistent with a propagating rupture. This means that the early arrival of secondary phases can prevent an image of the entire rupture. Furthermore, the location of the ISNet in nearly the strike direction impedes a reliable detection of possible bilateral rupture because the two source signals would overlap.

For the L'Aquila mainshock, our image shows a rupture of 17-km length, which propagates unilaterally from northwest to southeast with an average velocity of about

3 km/s. Propagation direction and rupture length agree with the moment distribution along the fault strike from FMNEAREG (Fig. 6a) and with local strong-motion and Global Positioning System data (Cirella *et al.*, 2009). Also, the general distribution of observed macroseismic intensities (Camassi *et al.*, 2009) supports the directivity toward the southeast (background color in Fig. 6c). The rupture velocity of 3 km/s is significantly higher than our estimate of 2.2 km/s from *S*-wave displacement spectra. Inserting $v_r = 3$ km/s in equation 4 would yield a corner frequency around 1.5 Hz, which clearly contradicts the observed *S*-wave displacement spectra (Fig. 4). Alternatively, an unrealistic fault length of more than 75 km would be required with $v_r = 3$ km/s to result in our estimate of $f_c = 0.33$ Hz. Also Cirella *et al.* (2009) found an along-strike rupture velocity of 2.2 km/s. However, equation 4 is just an order of magnitude estimate with a very simple directivity model behind it. To this end, we do not have a convincing explanation for the possibly overestimated rupture velocity from beamforming. It might be related to an incomplete rupture image and a trade-off between imaged source location and time. We plan to apply an imaging technique to the local RAN acceleration records with the aim of obtaining an improved rupture image.

Nevertheless, our individual results for source parameters of the L'Aquila earthquake are mostly consistent and are within the range of values obtained in other studies with different datasets. The work presented here demonstrates that the use of array techniques, and a dense accelerometer network can provide quick and robust estimates of source parameters of moderate-sized earthquakes located outside the network. We also propose to apply and evaluate the described procedures at other dense accelerometer networks.

Data and Resources

The seismic waveforms used in this study are available for download from the ISNet <http://isnet.na.infn.it/cgi-bin/isnet-events/isnet.cgi> (Event 14196r). Data from the RAN network are available in the Italian Accelerometric Archive (ITACA) at <http://itaca.mi.ingv.it/ItacaNet>. For standard seismic data processing, we used the Seismic Analysis Code software, which can be requested from the Incorporated Research Institutions for Seismology (<http://www.iris.edu>). The ISOLA code (Sokos and Zahradnik, 2008) is an open-access software available at <http://seismo.geology.upatras.gr/isola/>. We implemented multichannel processing with the open source CWP/SU Seismic Unix package (<http://www.cwp.mines.edu/cwpcodes/>; Cohen and Stockwell, 2008) and generated most figures with the Generic Mapping Tools Release 4.3.1 (<http://gmt.soest.hawaii.edu>; Wessel and Smith, 1998). Web pages were last accessed on 5 November 2010.

Acknowledgments

We thank Jiri Zahradnik and an anonymous reviewer for their constructive comments. This study was financially supported by the Italian Depart-

ment of Civil Protection (DPC) and the Istituto Nazionale di Geofisica e Vulcanologia (INGV) within the research framework programs S5 and S3. ISNet station corrections were provided by Emanuela Matrullo.

References

- Aki, K., and P. G. Richards (1980). *Quantitative Seismology*, Vol. 1, W. H. Freeman, San Francisco, 512 pp.
- Amato, A., and F. M. Mele (2008). Performance of the INGV National Seismic Network from 1997 to 2007, *Ann. Geophys.* **51**, no. 2–3, 417–431.
- Anderson, J. G., and S. E. Hough (1984). A model for the shape of the Fourier amplitude spectrum of acceleration at high frequencies, *Bull. Seismol. Soc. Am.* **74**, no. 5, 1969–1993.
- Bagh, S., L. Chiaraluce, P. De Gori, M. Moretti, A. Govoni, C. Chiarabba, P. Di Bartolomeo, and M. Romanelli (2007). Background seismicity in the Central Apennines of Italy: The Abruzzo region case study, *Tectonophysics* **444**, no. 1–4, 80–92, doi [10.1016/j.tecto.2007.08.009](https://doi.org/10.1016/j.tecto.2007.08.009).
- Beeler, N. M., T. F. Wong, and S. H. Hickman (2003). On the expected relationships among apparent stress, static stress drop, effective shear fracture energy, and efficiency, *Bull. Seismol. Soc. Am.* **93**, no. 3, 1381–1389, doi [10.1785/0120020162](https://doi.org/10.1785/0120020162).
- Boatwright, J. (1980). A spectral theory for circular seismic sources; simple estimates of source dimension, dynamic stress drop, and radiated seismic energy, *Bull. Seismol. Soc. Am.* **70**, no. 1, 1–27.
- Boatwright, J. (1984). Seismic estimates of stress release, *J. Geophys. Res.* **89**, no. B8, 6961–6968, doi [10.1029/JB089iB08p06961](https://doi.org/10.1029/JB089iB08p06961).
- Bobbio, A., M. Vassallo, and G. Festa (2009). A local magnitude scale for southern Italy, *Bull. Seismol. Soc. Am.* **99**, no. 4, 2461–2470, doi [10.1785/0120080364](https://doi.org/10.1785/0120080364).
- Bouchon, M. (1981). A simple method to calculate Green's functions for elastic layered media, *Bull. Seismol. Soc. Am.* **71**, no. 4, 959–971.
- Camassi, R., R. Azzaro, F. Bernardini, S. D'Amico, E. Ercolani, A. Rossi, A. Tertulliani, M. Vecchi, and P. Galli (2009). Macroseismic survey of the April 6, 2009 L'Aquila earthquake (central Italy), *Eos Trans. AGU*, **90**, Fall Meet. Suppl., abstract U23A-0025.
- Cirella, A., A. Piatanesi, M. Cocco, E. Tinti, L. Scognamiglio, A. Michelini, A. Lomax, and E. Boschi (2009). Rupture history of the 2009 L'Aquila (Italy) earthquake from non-linear joint inversion of strong motion and GPS data, *Geophys. Res. Lett.* **36**, no. 19, L19304, doi [10.1029/2009GL039795](https://doi.org/10.1029/2009GL039795).
- Cohen, J. K., and J. W. Stockwell (2008). CWP/SU: Seismic Unix Release No. 41: An open source software package for seismic research and processing, Center for Wave Phenomena, Colorado School of Mines, Golden, Colorado, <http://www.cwp.mines.edu/cwpcodes/>.
- Delouis, B., C. Charlety, and M. Vallée (2008). Fast determination of earthquake source parameters from strong motion records: M_w , focal mechanism, and slip distribution, in EGU General Assembly, *Geophys. Res. Abstr.* **10**, abstract 04939.
- Delouis, B., J. Charlety, and M. Vallée (2009). A method for rapid determination of moment magnitude M_w for moderate to large earthquakes from the near-field spectra of strong-motion records (MWSYNTH), *Bull. Seismol. Soc. Am.* **99**, no. 3, 1827–1840, doi [10.1785/0120080234](https://doi.org/10.1785/0120080234).
- Di Luccio, F., G. Ventura, R. Di Giovambattista, A. Piscini, and F. R. Cinti (2010). Normal faults and thrusts re-activated by deep fluids: The 6 April 2009 M_w 6.3 L'Aquila earthquake, central Italy, *J. Geophys. Res.* **115**, no. B06315, doi [10.1029/2009JB007190](https://doi.org/10.1029/2009JB007190).
- Frohlich, C., and J. Pulliam (1999). Single-station location of seismic events: A review and a plea for more research, *Phys. Earth Planet. In.* **113**, no. 1–4, 277–291, doi [10.1016/S0031-9201\(99\)00055-2](https://doi.org/10.1016/S0031-9201(99)00055-2).
- Galadini, F., and P. Galli (1999). The Holocene paleoearthquakes on the 1915 Avezzano earthquake faults (central Italy): Implications for active tectonics in the central Apennines, *Tectonophysics* **308**, no. 1–2, 143–170, doi [10.1016/S0040-1951\(99\)00091-8](https://doi.org/10.1016/S0040-1951(99)00091-8).
- Huber, P. J. (1964). Robust estimation of a location parameter, *Ann. Math. Stat.* **35**, no. 1, 73–101, doi [10.1214/aoms/1177703732](https://doi.org/10.1214/aoms/1177703732).

- Hutton, L. K., and D. M. Boore (1987). The M_L scale in southern California, *Bull. Seismol. Soc. Am.*, **77**, no. 6, 2074–2094.
- Ide, S., and G. C. Beroza (2001). Does apparent stress vary with earthquake size?, *Geophys. Res. Lett.* **28**, no. 17, 3349–3352, doi [10.1029/2001GL013106](https://doi.org/10.1029/2001GL013106).
- Ishii, M., P. M. Shearer, H. Houston, and J. E. Vidale (2005). Extent, duration and speed of the 2004 Sumatra-Andaman earthquake imaged by the Hi-Net array, *Nature* **435**, 933–936, doi [10.1038/nature03675](https://doi.org/10.1038/nature03675).
- Krüger, F., and M. Ohrnberger (2005). Tracking the rupture of the $M_w = 9.3$ Sumatra earthquake over 1,150 km at teleseismic distance, *Nature* **435**, 937–939, doi [10.1038/nature03696](https://doi.org/10.1038/nature03696).
- Li, H., A. Michelini, L. Zhu, F. Bernardi, and M. Spada (2007). Crustal velocity structure in Italy from analysis of regional seismic waveforms, *Bull. Seismol. Soc. Am.* **97**, no. 6, 2024–2039, doi [10.1785/0120070071](https://doi.org/10.1785/0120070071).
- Madariaga, R. (1976). Dynamics of an expanding circular fault, *Bull. Seismol. Soc. Am.* **66**, no. 3, 639–666.
- Madariaga, R. (1977a). Implications of stress-drop models of earthquakes for the inversion of stress drop from seismic observations, *Pure Appl. Geophys.* **115**, no. 1, 301–316, doi [10.1007/BF01637111](https://doi.org/10.1007/BF01637111).
- Madariaga, R. (1977b). High-frequency radiation from crack (stress drop) models of earthquake faulting, *Geophys. J. R. Astr. Soc.* **51**, no. 3, 625–651, doi [10.1111/j.1365-246X.1977.tb04211.x](https://doi.org/10.1111/j.1365-246X.1977.tb04211.x).
- Marquardt, D. W. (1963). An algorithm for least-squares estimation of nonlinear parameters, *SIAM J. Appl. Math.* **11**, no. 2, 431–441, doi [10.1137/0111030](https://doi.org/10.1137/0111030).
- Neidell, N., and M. T. Taner (1971). Semblance and other coherency measures for multichannel data, *Geophysics* **36**, no. 3, 482–497, doi [10.1190/1.1440186](https://doi.org/10.1190/1.1440186).
- Rost, S., and C. Thomas (2002). Array seismology: Methods and applications, *Rev. Geophys.* **40**, no. 3, 1008, doi [10.1029/2000RG000100](https://doi.org/10.1029/2000RG000100).
- Schweitzer, J. (2001). HYPOSAT—An enhanced routine to locate seismic events, *Pure Appl. Geophys.* **158**, no. 1–2, 277–289, doi [10.1007/PL00001160](https://doi.org/10.1007/PL00001160).
- Snoke, J. A. (1987). Stable determination of (Brune) stress drops, *Bull. Seismol. Soc. Am.* **77**, no. 2, 530–538.
- Sokos, E. N., and J. Zahradník (2008). ISOLA a Fortran code and a Matlab GUI to perform multiple-point source inversion of seismic data, *Comp. Geosci.* **34**, no. 8, 967–977, doi [10.1016/j.cageo.2007.07.005](https://doi.org/10.1016/j.cageo.2007.07.005).
- Walters, R. J., J. R. Elliott, N. D’Agostino, P. C. England, I. Hunstad, J. A. Jackson, B. Parsons, R. J. Phillips, and G. Roberts (2009). The 2009 L’Aquila earthquake (central Italy): A source mechanism and implications for seismic hazard, *Geophys. Res. Lett.* **36**, no. 17, L17312, doi [10.1029/2009GL039337](https://doi.org/10.1029/2009GL039337).
- Weber, E., V. Convertito, G. Iannaccone, A. Zollo, A. Bobbio, L. Cantore, M. Corciulo, M. Di Crosta, L. Elia, C. Martino, A. Romeo, and C. Satriano (2007). An advanced seismic network in the southern Apennines (Italy) for seismicity investigations and experimentation with earthquake early warning, *Seismol. Res. Lett.* **78**, no. 6, 622–634, doi [10.1785/gssrl.78.6.622](https://doi.org/10.1785/gssrl.78.6.622).
- Wells, D. L., and K. J. Coppersmith (1994). New empirical relationships among magnitude, rupture length, rupture width, rupture area, and surface displacement, *Bull. Seismol. Soc. Am.* **84**, no. 4, 974–1002.
- Wessel, P., and W. H. F. Smith (1998). New, improved version of generic mapping tools released, *EOS Trans. AGU* **79**, 579.
- Wyss, M. (1970). Apparent stresses of earthquakes on ridges compared to apparent stresses of earthquakes in trenches, *Geophys. J. R. Astr. Soc.* **19**, no. 5, 479–484, doi [10.1111/j.1365-246X.1970.tb00153.x](https://doi.org/10.1111/j.1365-246X.1970.tb00153.x).
- Zahradník, J., F. Gallovič, E. Sokos, A. Serpetsidaki, and A. Tselentis (2008). Quick fault-plane identification by a geometrical method: Application to the M_w 6.2 Leonidio earthquake, 6 January 2008, Greece, *Seismol. Res. Lett.* **79**, no. 5, 653–662, doi [10.1785/gssrl.79.5.653](https://doi.org/10.1785/gssrl.79.5.653).
- Dipartimento di Scienze Fisiche
Unità di Ricerca in Sismologia Sperimentale e Computazionale
Università degli Studi di Napoli Federico II
Complesso Universitario Monte S. Angelo, via Cintia
80126 Napoli, Italy
(N.M., A.Z., A.O., G.F., A.E.)
- Dipartimento di Studi Geologici e Ambientali
Università degli Studi del Sannio
82100 Benevento, Italy
(R.D.)
- GeoAzur—Observatoire de la Côte d’Azur
Centre National de la Recherche Scientifique—Université de Nice Sophia
Antipolis
250, Rue Albert Einstein
06560 Valbonne, France
(B.D.)
- Istituto Nazionale di Geofisica e Vulcanologia
Osservatorio Vesuviano via Diocleziano 328
80124 Napoli, Italy
(A.B.)